The Cryosphere
Discussions

Simultaneous estimation of wintertime sea ice thickness and snow depth from space-borne freeboard measurements

Hoyeon Shi[1], Byung-Ju Sohn[1], Gorm Dybkjær[2], Rasmus Tage Tonboe[2], Sang-Moo Lee[1,3,4]

[1]School of Earth and Environmental Sciences, Seoul National University, Seoul, Republic of Korea
[2]Danish Meteorological Institute, Copenhagen, Denmark
[3]Center for Environmental Technology, ECEE, University of Colorado-Boulder, Boulder, Colorado, USA
[4]National Snow and Ice Data Center, CIRES, University of Colorado-Boulder, Boulder, Colorado, USA

Correspondence to: Byung-Ju Sohn (sohn@snu.ac.kr)

Abstract. A method of simultaneously estimating snow depth and sea ice thickness using satellite-based freeboard measurements over the Arctic Ocean during winter was proposed. The ratio of snow depth to ice thickness (referred to as α) was defined and used in constraining the conversion from the freeboard to ice thickness in satellite altimetry. Then, α was empirically determined using the ratio of temperature difference of the snow layer to the difference of the ice layer, to allow the determination of α from satellite-derived snow surface temperature and snow–ice interface temperature. The proposed method was validated against NASA's Operation IceBridge measurements, and comparison results indicated that the algorithm adequately retrieves snow depth and ice thickness simultaneously: retrieved ice thickness was found to be better than the current satellite retrieval methods relying on the use of snow depth climatology as input, in terms of mean bias and RMSE. The application of the proposed method to CryoSat-2 ice freeboard measurements yields similar results. In conclusion, the developed α-based method has the capacity to derive ice thickness and snow depth, without relying on the snow depth information as input to the buoyancy equation for converting freeboard to ice thickness.

1 Introduction

Satellite altimeters have been used to estimate sea ice thickness for nearly two decades (Kwok et al., 2009; Laxon et al., 2013). The altimeters do not measure sea ice thickness directly but measure the sea ice freeboard which is then converted to sea ice thickness with assumptions, for example, regarding the snow depth, snow/ice densities, and radar penetration (Ricker et al., 2014). We hereafter refer to this procedure as 'freeboard to thickness conversion'.

Generally used two types of satellite altimeters measure different sea ice freeboards. Lidar altimeters such as NASA's ICESat (Zwally et al., 2002) and ICESat-2 (Markus et al., 2017) missions measure total freeboard (h_{tf}): the height from the sea surface to the snow surface. On the other hand, radar altimeters such as ESA's CryoSat-2 (CS2) (Wingham et al., 2006) measure radar freeboard (h_{rf}): the height from the sea surface to radar scattering horizon. Several studies indicate that the radar scattering horizon is at or above the snow–ice interface depending on ice type and snow/ice conditions (Armitage and Ridout, 2015; Tonboe et al. 2010). However, the radar scattering horizon is often treated as the snow–ice interface (Kurtz et

al., 2014; Kwok and Cunningham, 2015). The height from the sea surface to the snow–ice interface is called ice freeboard (h_f). The three different freeboards are indicated in Fig. 1.

For both lidar and radar altimeters, snow depth (h) is required as an input to constrain the freeboard to thickness conversion; thus, the conversion results are highly dependent on snow depth (Ricker et al., 2014; Zygmuntowska et al., 2014; Kern et al.

35 2015). The buoyancy equation used in the freeboard to thickness conversion describes the balance between buoyancy and the weight of snow and ice. For given freeboard and snow/ice densities, sea ice thickness (H) is a function of h. According to Zygmuntowska et al. (2014), up to 70% of uncertainty in the freeboard to thickness conversion stems from the poorly constrained snow depth. However, mapping the Arctic scale snow depth distribution is challenging. The most commonly used snow depth information necessary for the freeboard to thickness conversion is the modified version of the snow depth

40 climatology by Warren et al. (1999) (hereafter W99). W99 is based on in-situ measurements at Soviet drifting stations (1954–1991) mostly on multi-year ice (MYI). Kurtz and Farrell (2011) compared W99 with Operation IceBridge (OIB) snow depth measurements in 2009 and claimed that W99 was still valid on the MYI region and significantly differed from OIB snow depth on first-year ice (FYI). Based on that study, Modified W99 (hereafter MW99) was developed, which halves W99 snow depth in regions covered by FYI. MW99 is often used in CS2 ice thickness products available at CPOM-UCL

45 (Laxon et al., 2013), AWI (Ricker et al., 2014), and NSIDC (Kurtz et al., 2017).

However, the use of MW99 for freeboard to thickness conversion understandably yields a substantial error, considering that W99 is a climatology. This is because the actual snow depth distribution is subject to the year-to-year variation of snow–ice system, thus the climatology based on the 37-year measurements of snow depth would deviate significantly from the actual distribution (Webster et al., 2014). Accordingly, such deviation causes errors in the estimation of ice thickness. Thus,

50 additional snow observations covering both MYI and FYI on the Arctic basin scale would be ideal as a replacement of MW99.

There have been various approaches aimed at obtaining the snow depth distribution over the Arctic scale using satellite observations. Markus and Cavalieri (1998) developed an algorithm based on the Brightness Temperatures (TBs) of Special Sensor Microwave/Imager (SSM/I) based on the negative correlation of the snow depth with the spectral gradient ratio

55 between 18 and 37 GHz of vertically polarized TB's on the Antarctic FYI. Comiso et al. (2003) have updated the coefficients of this algorithm for the Advanced Microwave Scanning Radiometer for EOS (AMSR-E). However, snow depth retrieval using this algorithm is relatively less accurate when the MYI fraction within the grid cell is significant (Brucker and Markus, 2013). Recently, Rostosky et al. (2018) suggested a new method: using the lower frequency pair of 7 and 19 GHz to overcome the limitation. Nonetheless, estimating the basin-scale distribution seems to be a difficult task.

60 There are other approaches involving the use of the lower frequency measurements at L-band. Using Soil Moisture Ocean Salinity (SMOS) measurements, Maaß et al. (2013) found that 1.4 GHz TB depends on the snow depth through the insulation effect of snow layer, and they determined snow depth by matching RTM simulated TBs with SMOS-measured TBs. Zhou et al. (2018) simultaneously estimated the sea ice thickness and snow depth by adding additional laser altimeter

freeboard information, improving the Maaß et al. (2013) approach. However, both of these RTM-based approaches require a

65   priori information on ice properties (e.g. temperature and salinity profiles).

Other approaches worth mentioning are snow depth retrieval using dual-frequency altimetry (Guerreiro et al., 2016; Lawrence et al., 2018, Kwok and Markus, 2018), snow on sea ice model accumulating snowfall from reanalysis (Petty et al., 2018), multilinear regression (Kilic et al., 2019), and the neural network approach (Braakmann-Folgmann and Donlon, 2019). However, these methods do not satisfactorily meet the criteria required for freeboard to ice conversion over the entire Arctic

70   Ocean basin scale or multi-year time scale.

In this situation, let us switch our point of view to solving the buoyancy equation instead of retrieving snow depth. Remember that there is one buoyancy equation with two unknowns (snow depth and ice thickness) for given densities and freeboard. The attempt so far has been to add one constraint (snow depth information) to the buoyancy equation for solving ice thickness. However, if a particular relationship between two unknowns is available, it can be used to constrain the

75   equation yielding both ice thickness and snow depth.

To identify such a relationship, this study examines the vertical thermal structure within the snow/ice layers observed by drifting buoys. The vertical thermal structure of a snow–ice system in winter is rather simple; the temperature profile of the snow–ice system can be assumed to be piecewise linear, as illustrated in Fig. 1. Therefore, the temperatures at three interfaces can represent the thermal state of the snow–ice system fairly well; they are (1) air–snow interface temperature (T_{as}),

80   (2) snow–ice interface temperature (T_{si}), and (3) ice–water interface temperature (T_{iw}). T_{iw} is assumed to be almost constant at the freezing temperature of seawater (Maaß et al., 2013), implying that two other interface temperatures (T_{as} and T_{si}) are sufficient to describe the thermal structure of the system.

Based on this thermal structure, there may exist a constraint relating the snow depth and ice thickness. In identifying a constraint, conductive heat flux is assumed to be continuous through the snow–ice interface (Maykut and Untersteiner, 1971),

85   implying that conductive heat fluxes within the snow and ice layers are same under the steady-state assumed in the given thermal structure. As the conductive heat flux is proportional to the bulk temperature difference of the layer divided by its thickness, it is possible to deduce the relationship between snow depth and ice thickness from the given thermal structure.

Once the relationship is obtained, then it is possible to apply it to the Arctic Ocean basin scale because the thermal structure can be resolved from satellites, as shown in the recently available basin-scale and long-term satellite-derived interface

90   temperatures (Dybkjær et al., 2020; Lee et al., 2018). In determining snow depth along with ice thickness, instead of using the snow depth as an input to solve for the ice thickness, we intend to (1) examine the relationship between the vertical thermal structure of a snow–ice system (T_{as} and T_{si}) and the thicknesses of the snow and ice layer (h and H) using buoy measurements, (2) retrieve sea ice thickness and snow depth simultaneously by applying their relationship to the freeboard to thickness conversion as a constraint, thus replacing the snow depth information. The result may reduce uncertainty in the

95   freeboard to ice thickness conversion by replacing the currently used snow depth information.

2 Method

Here, we provide the theoretical background of how the snow–ice thickness ratio ($\alpha = h / H$) can be related to T_{as} and T_{si}. Then, after empirically determining the relationship of α to T_{as} and T_{si} from buoy measured temperature profiles, α obtained from satellite-observed T_{as} and T_{si} is used to constrain the conversion from freeboard to ice thickness over the Arctic Ocean

100   during winter.

2.1 Theoretical background

We intend to find a relationship between snow depth and ice thickness in terms of the vertical thermal structure of a snow–ice system. Because the temperature gradient within the snow and ice layer is linked to both temperature and thickness, we focus on the temperature gradient. Owing to the physical reasoning that the conductive heat flux is continuous across the

105   snow–ice interface (Maykut and Untersteiner, 1971), the following relationship is valid at the snow–ice interface:

$$k_{snow} \left. \frac{\partial T_{snow}}{\partial z} \right|_{z=0} = k_{ice} \left. \frac{\partial T_{ice}}{\partial z} \right|_{z=0} \tag{1}$$

In Eq. (1), the subscripts *snow* and *ice* denote their respective layers while T, k, and z denote temperature, thermal conductivity, and depth, respectively. The snow–ice interface is defined as $z = 0$. Assuming a piecewise linear temperature profile within the snow–ice layer, Eq. (1) can be rewritten as follows:

110    $$k_{snow} \frac{T_{as} - T_{si}}{h} = k_{ice} \frac{T_{si} - T_{iw}}{H} \tag{2}$$

where subscripts *as*, *si*, and *iw* denote the air–snow, snow–ice, and ice–water interface, respectively, and H and h denote the sea ice thickness and snow depth as in Fig. 1. Introducing a variable α, which is the snow–ice thickness ratio, Eq. (2) becomes:

$$\alpha = \frac{h}{H} = \frac{k_{snow}}{k_{ice}} \frac{\Delta T_{snow}}{\Delta T_{ice}} \tag{3}$$

115   Here, ΔT denotes the temperature difference between the top and bottom of each snow or ice layer (i.e. $\Delta T_{snow} = T_{as} - T_{si}$, $\Delta T_{ice} = T_{si} - T_{iw}$). As explained in detail in Sect. 2.3, α can be used to constrain the freeboard to thickness conversion. Thus, once α is known, both snow depth and ice thickness can be simultaneously estimated from altimeter-measured freeboard, instead of using snow depth data for ice thickness retrieval.

2.2 Empirical determination of 'α-prediction equation' from buoy measurements

120   To obtain α, the conductivity ratio (k_{snow}/k_{ice}) should be known even if the temperature difference ratio ($\Delta T_{snow}/\Delta T_{ice}$) is given. In this study, instead of using the conventional conductivity ratio found in literature, it is empirically determined using buoy-

measured α and $\Delta T_{snow}/\Delta T_{ice}$. Thus, the interface should be defined and determined from buoy-measured temperature profiles, which show a piecewise linear temperature profile as shown in Fig. 1.

The buoy-measured temperature profiles in the vertical resolution of 10 cm are used in this study (Sect. 3.1). Although the

125 instrument initially sets the zero-depth reference position to be approximately at the snow–ice interface, the reference position can deviate from the initial location if the ice deforms, or if the snow refreezes after the temporary melt. In addition, the interfaces (air–snow, snow–ice, and ice–water) may be located in between measurement levels in a 10 cm spacing. Therefore, the interface searching algorithm is developed to determine three interfaces (y_{as}, y_{si}, y_{iw}) and their respective temperatures (T_{as}, T_{si}, T_{iw}) by extrapolating each piecewise linear temperature profile iteratively.

130 The interface searching algorithm iterates three processes to find the location and temperature of each interface: it (1) divides temperature profile into four layers using the most recently available locations of the three interfaces, (2) finds a linear regression line of temperature profile at each layer, and (3) updates the location and temperature of each interface by finding an intersection between two adjacent regression lines. The algorithm fails if the temperature profile is far from linear, or the thickness of a certain layer is thin to have less than two data points. More detailed procedures for determining the interface

135 are provided in Fig. 2, as a flow chart. The outputs are T_{as}, T_{si}, T_{iw}, H (= y_{as} - y_{si}), and h (= y_{si} - y_{iw}). Examples of the interface searching results for 15-day averaged temperature profiles are shown in Fig. 3. The algorithm works adequately for both CRREL-IMB (Fig. 3a–c) and SHEBA buoys (Fig. 3d–f). For the analysis, temperature profiles are used only if T_{as} is colder than T_{si}. As the analysis period is winter, there are very few discarded profiles when this criterion is applied.

As T_{as}, T_{si}, T_{iw}, H, and h can be obtained from the previous interface determination with buoy data, the calculation of

140 $\Delta T_{snow}/\Delta T_{ice}$ and α becomes straight forward. Then, an empirical relationship can be obtained by relating α to $\Delta T_{snow}/\Delta T_{ice}$ by running a regression model, and details are given in Sect. 4. However, for the time being, we assume that the regression equation (referred to as an 'α-prediction equation' that will be discussed in Sect. 4) is used to predict α from $\Delta T_{snow}/\Delta T_{ice}$.

2.3 Simultaneous estimation of ice thickness and snow depth from satellite-based freeboard using α

In this section, we describe how α can be used to constrain the freeboard to thickness conversion. Based on the assumed

145 hydrostatic balance, ice thickness can be obtained from satellite-borne total freeboard or ice freeboard as follows:

$$H = h_{tf} \left(\frac{\rho_{water}}{\rho_{water} - \rho_{ice}} \right) - h \left(\frac{\rho_{water} - \rho_{snow}}{\rho_{water} - \rho_{ice}} \right) \tag{4}$$

$$H = h_f \left(\frac{\rho_{water}}{\rho_{water} - \rho_{ice}} \right) + h \left(\frac{\rho_{snow}}{\rho_{water} - \rho_{ice}} \right) \tag{5}$$

h_{tf} and h_f are the total freeboard and ice freeboard, and ρ denotes the density. With the use of α, defined in Eq. (3), Eqs. (4) and (5) become

150 $$H = h_{tf} \frac{\rho_{water}}{\rho_{water} - \rho_{ice} + \alpha(\rho_{water} - \rho_{snow})} \tag{6}$$

$$H = h_f \frac{\rho_{water}}{\rho_{water} - \rho_{ice} - \alpha \rho_{snow}} \tag{7}$$

From Eqs. (3)–(7), it is evident that snow depth and ice thickness can be simultaneously estimated from freeboards once α and ρ are known.

In order to obtain α from satellite measurements of T_{as} and T_{si}, we need to calculate the temperature difference ratio

155 ($\Delta T_{snow}/\Delta T_{ice}$). For the calculation, T_{iw} is set to be -1.5 °C. The freezing temperature of seawater is often assumed to be -1.8 °C; however, the value of -1.5 °C is chosen based on the buoy observations. Nevertheless, a sensitivity test indicated that the influence of a 0.3 °C difference in the freezing temperature on α was negligible. α values are calculated only at the pixel whose monthly sea ice concentration (SIC) is greater than 98% and rejected if T_{as} is warmer than T_{si}. The densities are prescribed with those used for OIB data processing: ρ_{snow}, ρ_{ice}, and ρ_{water} are 320 kg m^{-3}, 915 kg m^{-3}, and 1024 kg m^{-3},

160 respectively. Although ρ_{snow} varies seasonally (Warren et al., 1999) and ρ_{ice} is greater in MYI than in FYI (Alexandrov et al., 2010), we use the same densities as those of OIB data because we intend to compare outputs against OIB data. In solving Eq. (7), cases showing negative ice thickness ($\alpha > 0.341$ for the given densities) are rejected.

Before the Arctic basin-scale retrieval, ice thickness is estimated from OIB total freeboard measurement using Eq. (6), and from OIB-derived ice freeboard (Sect. 3.3) using Eq. (7), using satellite-derived α as a constraint. At the same time, the

165 corresponding snow depth is derived by multiplying obtained sea ice thickness and α. Sea ice thicknesses converted from MW99 using Eqs. (4) and (5) are also compared to examine how simultaneous retrievals might be compared with ICESat and CS2 retrieval of ice thickness. To differentiate various outputs, obtained snow depth and ice thickness are expressed with nomenclature such as '[constraint + freeboard source]'. For example, snow depth from α and OIB total freeboard is referred to as 'h [α + h_{tf} (OIB)]', and sea ice thickness from the MW99 snow depth and OIB ice freeboard is referred to as 'H [h

170 (MW99) + h_f (OIB)]'. Finally, ice thickness and snow depth are estimated from CS2 ice freeboard (Sect. 3.4) over the Arctic Ocean.

3 Data

Here, we provide detailed information on the data sets used for development of the retrieval algorithm, validation, and application to the Arctic ocean basin scale.

175 ### 3.1 CRREL and SHEBA buoy data

To determine the empirical relationship between α and $\Delta T_{snow}/\Delta T_{ice}$ using Eq. (3), we need information regarding h, H, T_{as}, T_{si}, and T_{iw} (as depicted in Fig. 1). These are sourced from temperature profiles observed by buoys deployed over the Arctic, as parts of the Surface Heat Energy Budget of the Arctic (SHEBA) campaign (Perovich et al., 2007) and the Cold Regions Research and Engineering Laboratory Ice Mass Balance (CRREL-IMB) buoy program (Perovich et al., 2019). Those buoy

180 observations are stored for further analysis if there is no missing value over the entire period ranging from November to March of the following year. Detailed information regarding ice types and initial snow/ice thicknesses at deployment locations are given in Table 1.

Time averages of temperature profiles are considered as inputs to the interface searching algorithm (described in Sect. 2.2) to meet the required near-equilibrium states (e.g. linear temperature profile). However, because of the possibility of results

185 depending on the averaging period, we examine the results by giving various averaging periods from one to 30 days.

3.2 Satellite-derived skin and interface temperatures

For applying the buoy-based α-prediction equation in retrieving the snow/ice thicknesses over the Arctic Ocean, satellite-derived T_{as} and T_{si} data are necessary. In this study, T_{as} is obtained from Arctic and Antarctic ice Surface Temperatures from thermal Infrared satellites sensors – version 2 (AASTI-v2) data (Dybkjær et al., 2020), and the monthly mean for the 1982–

190 2015 period is obtained from daily products. AASTI T_{as} is derived from CM SAF cLoud, Albedo and surface Radiation dataset from AVHRR data - Edition 2 (CLARA-A2) dataset (Karlsson et al., 2017), based on the algorithm described in Dybkjær et al. (2018). Information on the validation of this product is found in Dybkjær and Eastwood (2016). It is available in a 0.25° grid format, however, because other satellite data sets such as SIC are available in a 25 km Polar Stereographic SSM/I Grid, AASTI-v2 data are re-gridded in the same 25 km grid format. This reformatted AASTI-v2 data are called

195 'satellite skin temperature'.

T_{si} is obtained from Snow/Ice Interface Temperature (SIIT) produced by Lee et al. (2018) over 30 years (1988–2017) of wintertime (December to February) SSM/I and SSMIS Fundamental Climate Data Record of TBs (Berg et al., 2018). The daily data are in the 25 km grid format. It was reported that the satellite-derived T_{si} is consistent with snow–ice interface temperatures observed by CRREL-IMB buoys, with correlation coefficient, bias, and RMSE of 0.95, 0.15 K and 1.48 K,

200 respectively. In this study, we also include T_{si} for March for validating results against OIB data which are mostly collected during spring. Monthly composites are constructed by averaging daily data if data frequency is over 20. This product is called 'satellite interface temperature'.

3.3 OIB snow depth, total freeboard, and ice freeboard

In this study, OIB snow depth and total freeboard are used as a reference in the validation of snow depth and ice thickness

205 retrieved from the developed algorithm. NASA's OIB is an aircraft mission and it measures snow depth and total freeboard over the Arctic using the snow radar, Digital Mapping System (DMS), and Airborne Topographic Mapper (ATM) (Kurtz et al., 2013). Ice thickness is derived from measured snow depth and total freeboard, for the given snow and ice densities. In this study, ice freeboard is derived by subtracting the snow depth from the total freeboard.

The OIB data are available during the two months of March–April over the 2011–2015 period (Kurtz et al., 2015). Because

210 we use the November–March period for the buoy analysis, only March OIB data are considered for the validation. The OIB data are also reformatted into the 25 km grid format for comparison. If the location of one OIB individual data point falls

within a certain 25 km grid area, then the point data is binned in a corresponding grid. After completing the grid assignment, grid value is determined by calculating a simple arithmetic mean of all data within that grid area.

3.4 CS2 data

215 For examining the Arctic Ocean basin distribution of ice thickness and snow depth, CS2 freeboard measurement summary data are used (Kurtz et al., 2017). They are monthly mean composites of CS2 ice freeboard data in the 25 km Polar Stereographic SSM/I Grid format, covering the entire Arctic, and available from September 2010. Detailed descriptions of the retracker algorithm used in this dataset are found in the study by Kurtz et al. (2014). The data set also includes the sea ice thickness estimated from the use of MW99 snow depth as input to the conversion equation. Those ice thickness estimations

220 and MW99 snow depth values are used for purposes of comparison.

3.5 Sea ice concentration

Calculation of α is done over the pixel whose monthly SIC is greater than 98% (as described in Sect. 2.3). To determine pixels that meet this SIC criterion, 'bootstrap sea ice concentrations from Nimbus-7 SMMR and DMSP SSM/I-SSMIS version 3' produced by Comiso (2017) are used. This SIC dataset is provided in the 25-km Polar Stereographic SSM/I grid

225 format.

4 Results

4.1 The empirical relationship between α and $\Delta T_{snow}/\Delta T_{ice}$

We examine variables (i.e. T_{as}, T_{si}, T_{iw}, H, and h) obtained from buoy observations by applying the interface searching algorithm. In the scatter plot of weekly-averaged $\Delta T_{snow}/\Delta T_{ice}$ versus α (Fig. 4a), it appears that α linearly increases with

230 $\Delta T_{snow}/\Delta T_{ice}$ when the ratio is smaller than 1.8, but the linear slope becomes smaller when $\Delta T_{snow}/\Delta T_{ice}$ is larger than 1.8. This nature of slopes is found to be nearly invariant from year to year, as observed in different colors appearing in the entire range of $\Delta T_{snow}/\Delta T_{ice}$ of Fig. 4a. Also found is the consistent nature of the slopes even for different data sets; two different data sets (red points for SHEBA and other points for CRREL) covering various ranges of $\Delta T_{snow}/\Delta T_{ice}$, show similar distributions along two different slopes. Thus, it suffices to conclude that the slope change may not be due to different data sources or

235 different data periods.

Taking such changing slope with $\Delta T_{snow}/\Delta T_{ice}$ into account, we introduce a piecewise linear function that may express the slope change, i.e.:

$$y = \begin{cases} a_1 x + b_1 & x \le x_0 \\ a_2 x + b_2 & x > x_0 \end{cases}, \quad x_0 = \frac{b_1 - b_2}{a_2 - a_1} \tag{8}$$

In Eq. (8), x and y correspond to $\Delta T_{snow}/\Delta T_{ice}$ and α, respectively, and x_0 is the point where the slope transition takes place.

240 Applying Eq. (8) to data points from buoy-based variables, regression coefficients (a_1, b_1, a_2, b_2) and the transition point (x_0) in Eq. (8) are determined by minimizing the total variance - obtained regression line is plotted in Fig. 4a. α is predicted using the determined regression equation (hereafter referred to as α-prediction equation) and compared against original α values to see how well the regression was performed. The comparison of α with predicted values in Fig. 4b shows that the regression equation is well fitted because of the near-zero bias and 91.9% of explained variance.

245 Although the slope change discussed with Eq. (8) and Fig. 4 is based on the weekly averages, the nature of changing slope seems to be consistent among the data averaging periods except for a very short averaging period. Regressions given in the form of Eq. (8) are performed with buoy data averaged with different averaging periods to understand the nature of changing slope. Regression coefficients and transition point for the chosen averaging periods are examined, and results for four averaging periods are given in Table 2. Detailed information on the coefficients and associated statistics varying with the

250 averaging period is given in Fig. 5. The positions of slope change (x_0) are located at approximately 1.8, delineating a nearly invariant slope change, regardless of different data averaging periods. Fig. 5a shows that coefficients do not vary much with different averaging periods while coefficients of the first part of the regression line (a_1 and b_1, $x \leq x_0$) vary less than those of the second part (a_2 and b_2, $x > x_0$). The regression equations show that the explained variance (R^2) rises quickly when the averaging period is longer but levels off when data are averaged over a period that is longer than seven days. The bias

255 appears to be near zero over the various averaging periods. Thus, regression performance is found to be comparable if data are averaged over a period that is longer than a week. Further analysis of explanations of the possible causes of two slopes is found in Appendix A.

4.2 Validation against OIB estimates

According to the regression results, it is possible to estimate α from the $\Delta T_{snow}/\Delta T_{ice}$. Since the $\Delta T_{snow}/\Delta T_{ice}$ can be calculated

260 from the satellite skin and interface temperature (as described in Sect. 3.2), the corresponding α can be estimated from satellite measurements. Thus, we are able to simultaneously retrieve sea ice thickness and snow depth from altimeter-based freeboard measurements, following Eqs. (6) and (7). We test and validate this simultaneous retrieval approach using OIB data. Accordingly, ice thickness and snow depth are simultaneously estimated from OIB freeboard measurements and validated against the OIB snow depth (h (OIB)) and ice thickness (H (OIB)).

265 To calculate α, a data averaging period must be selected. Considering that the monthly composite of satellite freeboard measurements is needed to retrieve snow/ice thickness in the Arctic basin scale, it seems appropriate to use the monthly averaging period to calculate the monthly α distribution. Thus, we use the monthly averaged satellite temperatures and the coefficients for the 30-day averaging period (Table 2) to calculate α.

We simultaneously retrieved H and h for March of the 2011- 2015 period from the reformatted OIB freeboard measurements

270 (Sect. 3.3) together with satellite-derived α. As expressed in Eqs. (6) and (7), two different ice thickness retrievals are

possible, depending on the use of the freeboard type (i.e. total freeboard h_{tf} vs. ice freeboard h_f). Two accordingly associated retrievals of snow depth are available. Retrieved results of ice thickness (H) and snow depth (h) from the use of OIB total freeboard and ice freeboard are given in the first and second row of Fig. 6, respectively. Corresponding OIB measurements are given at the bottom of Fig. 6. The comparison between any snow/ice retrievals and OIB measurements appear to be consistent with each other for both snow depth and ice thickness, in terms of magnitudes and distribution.

To compare the results quantitatively, scatterplots of comparing retrievals against OIB measurements are made, along with statistics for the snow depth and ice thickness retrievals, in the top four panels of Fig 7. The top-two left panels are derived from the use of OIB total freeboard (h_{tf}) while the top-two right panels are derived from the OIB ice freeboard (h_f). The comparison is done only for pixels where all four products (i.e. snow/ice thicknesses from two different freeboards) are available. This indicates that the snow depth from the total freeboard (top left) is fairly consistent with the OIB snow depth, with a correlation coefficient of 0.73 and with a near-zero bias. The retrieved ice thickness from the total freeboard (middle left) appears to be consistent with OIB ice thickness, with a correlation coefficient of 0.93 and a bias around 2 cm. The RMSEs for snow depth and ice thickness are 6.8 cm and 44 cm, respectively. Based on the comparison results, Eq. (8) obtained from buoy measurements can be successfully implemented with space-borne total freeboard measurements for the simultaneous retrieval of snow depth and ice thickness.

Following Eq. (7), snow depth and ice thickness retrievals are made from the use of ice freeboard measurements, and results are presented in the top-two right panels in Fig. 7. The comparison of obtained ice thickness against the OIB ice thickness indicates that the retrieved ice thickness shows nearly the same quality as that retrieved from the total freeboard measurements. On the other hand, snow retrievals from the ice freeboard show more scattered features, compared with snow retrieval results from the total freeboard. More scattered features found in snow depth from the ice freeboard are likely due to the relatively more sensitive nature to the prescribed densities, as noted in Eq. (7). Note that Eq. (7) has a smaller denominator than that for Eq. (6).

Examining how the current practices of retrieving the sea ice thickness through ICESat and CS2 measurements are compared with the simultaneous retrievals is of interest. In doing so, OIB-measured total freeboard and ice freeboard are converted into ice thickness using MW99 as input to solve Eqs. (4) and (5). These two ice thickness retrievals are referred to as ICESat-like thickness and CS2-like thickness, respectively, and their comparisons are now observed in two panels at the bottom of Fig. 7. Apparently, ICESat-like thickness tends to underestimate the ice thickness by about 50 cm when MW99 is used, in comparison to OIB thickness. On the other hand, CS2-like ice thickness shows an overestimate of about 23 cm. Nevertheless, their correlation coefficients and RMSEs are similar to the results obtained from the α method.

The different direction of the bias between ICESat-like and CS2-like thicknesses is thought to be attributable to the snow depth error according to Eqs. (4) and (5). Therefore, if there are decreasing trends in both ice thickness and snow depth, the decreasing trend of ice thickness estimated from the constant snow depth will be diminished in radar, while being amplified in lidar. Because of this, the construction of the ice thickness (or volume) trend from the two different satellite altimeters would be problematic if MW99 snow depth is used for the freeboard to thickness conversion. For example, it would be hard

305 to compare the sea ice thickness records estimated from ICESat and CS2 observations and to extend the current ice thickness
record from CS2 with recently launched NASA's ICESat-2 which carries a lidar altimeter, for the same reason.

4.3 Simultaneous retrieval of ice thickness and snow depth from CS2 measurements

We have demonstrated that the method of simultaneously retrieving the sea ice thickness and snow depth was successfully
implemented with OIB measurements. Now we extend the proposed approach to satellite freeboard measurements. Here, the
310 method is tested with CS2 freeboard measurements, solving for H in Eq. (7), and α is obtained from the collocated satellite
skin and interface temperature data.

Monthly means of CS2-estimated freeboard (h_f), retrieved α, ice thickness (H) and snow depth (h) for December 2013 to
March 2014 are given in Fig. 8. The geographical distribution of α indicates that α is largest in January and becomes smaller
in the following months. Geographically, there seems to be no coherent distribution of α between months, although
315 interestingly the lowest α values are always found over the north of the Canadian Archipelago and the western part of the
Arctic Ocean shows α that is generally larger than that over the eastern part.

Retrieved ice thickness from the CS2 freeboard (h_f) using obtained α is presented in the third row of Fig. 8. As expected, as
noted in Eq. (7), H shows a similar geographical distribution as shown in the freeboard (the first row). The thickest area is
located north of the Canadian Archipelago, where the ice appears thicker than 4 m. On the other hand, most of the FYI
320 thickness appears to range from 1.0 m to 2.0 m. The snow depth h is obtained by multiplying α by H (in 2nd and 3rd rows),
following Eq. (3), and results are given at the bottom. The obtained snow distribution indicates that thicker snow areas are
generally coincident with thicker MYI areas. Likewise, the thinner snow area coincides with the thinner FYI area. Such
similarity should be consistent with the notion that MYI should accumulate more precipitation than FYI because of its longer
existence.

325 The accuracies of CS2 retrievals using the current α approach can be indirectly tested against OIB measurements. We do so
by examining whether the relationship between H [$\alpha + h_f$ (OIB)] and H [h (MW99) + h_f (OIB)], in which each ice thickness
retrieval has its own accuracy against OIB measurements, can be reproduced in CS2-based retrievals. If similar results are
found, we can deduce respective accuracies against those found from the validation efforts against OIB measurements. The
relationship, which can be obtained from analysis in Fig. 7, is compared with the relationship found in the current results in
330 Fig. 8, (i.e., H [$\alpha + h_f$ (CS2)] and H [h (MW99) + h_f (CS2)]); the results are presented in Fig. 9. Observably, the relationship
from CS2 freeboard data (Fig. 9b) is very similar to the relationship obtained from the comparison results from OIB
measurements. This similarity of the slope strongly indicates that the CS2-based sea ice thickness from the current α method
has similar accuracy to that found in the validation against OIB measurements (Sect 4.2).

5. Conclusions and Discussion

335   A new approach towards simultaneously estimating snow depth and ice thickness from space-borne freeboard measurements was proposed and tested using OIB data and CS2 freeboard measurements. In developing the algorithm, the vertical temperature slopes were assumed to be linear within the snow and ice layers so that continuous heat flux could be maintained in both layers. This assumption allowed for the description of the snow–ice vertical thermal structure with snow skin temperature, snow–ice interface temperature, water temperature at the ice–water interface, snow depth, and ice

340 thickness. Based on the continuous heat transfer assumption, the snow–ice thickness ratio ($\alpha = h / H$) was introduced and could then be embedded into the freeboard to ice thickness conversion equations. Thus, information on both ice thickness and snow depth can be derived once α is known in case of the availability of a freeboard, without relying on the snow depth information as an input to the conversion from freeboard to ice thickness. From the drifting buoy measurements of temperature profile, snow depth, and ice thickness over the Arctic Ocean, we demonstrated that α can be reliably determined

345 using the ratio of the vertical difference of the snow-layer temperature to the vertical difference of ice-layer temperature ($\Delta T_{snow}/\Delta T_{ice}$). An empirical regression equation was obtained for predicting α from three interface temperatures.

  Before applying α-prediction equation to simultaneously retrieve the ice thickness and snow depth from satellite-borne freeboard measurements, the algorithm was validated using OIB measurements, in conjunction with satellite-derived snow skin temperature and snow–ice interface temperature. Validation results demonstrated that our proposed algorithm

350 adequately retrieved both parameters simultaneously. As a matter of fact, the ice thickness results were more accurate than they were from the current retrieval methods relying on the input of snow depth (this time MW99 snow climatology), in terms of mean bias and RMSE. It should be noted that in this case, snow depth is a retrieval product, instead of being input to the freeboard to ice thickness conversion adopted by CS2 or ICESat retrieval. Application was finally made for the retrieval of the snow depth and ice thickness from CS2 ice freeboard measurements from December 2013 to March 2014

355 using α as a constraint. Results showed that the quality of the obtained ice thickness was similar to that obtained from validation results against OIB measurements. Retrieved snow depth distributions were also found to be consistent with expectations.

  In the retrieval process, we may be concerned about the applicability of the algorithm developed with buoy observations representing the point circumstances, to the larger spatial and temporal scales that are inevitable in the satellite

360 measurements. This concern may be relevant upon observing the range of α values. α in the satellite's monthly and 25 km x 25 km spatial scales was found to be generally smaller than 0.2. The smaller range of α compared to that shown in the buoy analysis results is likely due to the scale differences, indicating that extreme α values often shown in buoy measurements (due to very thick snow and/or very thin ice) may never be observed in satellite measurements. However, the range may not be a problem because the relationship (Eq. (3)) expresses the thermal equilibrium condition described by temperature at three

365 interfaces, ratio of snow and ice thickness, and ratio of thermal conductivity between snow and ice. Considering that the algorithm is based on the equilibrium conditions, results should be valid regardless of spatial and temporal scales if the

prerequisite equilibrium conditions are met. Apparently, buoy observations contain so many different cases that equilibrium conditions are met with different thermal and physical conditions of snow–ice system. Sound validation results and the consistency between OIB and CS2 ice thickness retrieval results, which are subject to different scales, all suggest that point-
370   measured α-prediction equation can be applicable to satellite measurements.

Overall, the developed α-based method yields ice thickness and snow depth, without relying on a priori 'uncertain' snow depth information, which results in uncertainty in the ice thickness retrieval. The results that ice freeboard and the total freeboard yielded had nearly the same outputs when the α-approach was used. The proposed method is applicable to both lidar and radar altimeter data, although lidar-based altimeter data tend to offer relatively more suitable snow depth
375   information. We expect to continuously monitor the Arctic scale snow depth and ice thickness by applying the proposed α method to total freeboard observations by the recently launched ICESat-2, using temperature observations from the upcoming Meteorological Imager (MetImage) and Copernicus Imaging Microwave Radiometer (CIMR).

Appendix A: Physical interpretation of the piecewise linearity between α and $\Delta T_{snow}/\Delta T_{ice}$

The relationship found between α and $\Delta T_{snow}/\Delta T_{ice}$ showed a piecewise linearity, which is almost invariant with the data
380   averaging period. Because the slope change is neither attributable to different data sources nor different data periods, it is likely caused by the physical properties of snow and ice, as shown in Fig. A1. If the slope change is caused by the snow/ice condition, there will be a significant difference in snow/ice properties between the two parts showing different slopes. Here, we examine the possibility of different physical properties causing the difference in slopes. Through this comparison using buoy data, we may identify important properties that might be responsible for the piecewise linearity.
385   First, the mean of basic properties available from buoy measurements are compared. They include ice thickness, snow depth, snow–ice interface temperature, ice temperature ($T_{ice} = (T_{as} + T_{si}) / 2$), and so on. The comparison revealed that snow–ice system within the first part ($x \leq x_0$) is found to consist of relatively thicker ice (1.84 m), thinner snow (0.29 m), and colder ice (-9.13 °C) while the second part ($x > x_0$) is found to consist of relatively thinner ice (1.10 m), thicker snow (0.46 m), and warmer ice (-5.00 °C). In general, a thicker layer exhibits greater temperature difference within the layer. There is no
390   significant difference between the air–snow interface temperature (T_{as}) in the two parts.

The thermal conductivities, k_{snow} and k_{ice}, are also compared because what connects α and $\Delta T_{snow}/\Delta T_{ice}$ is the ratio of thermal conductivities. Before showing the results, we describe how to calculate k_{snow} and k_{ice}. First, the thermal conductivity ratio is calculated from buoy measured variables (i.e. T_{as}, T_{si}, T_{iw}, h, and H) using Eq. (3). Because the underlying physics in k_{snow} is significantly more complex, k_{ice} is estimated first and then k_{snow} is obtained by multiplying the calculated k_{ice} and k_{snow}/k_{ice}. To
395   calculate k_{ice}, the parameterization of Maykut and Untersteiner (1971), which describes k_{ice} as a function of salinity and temperature, is used.

$$k_{ice} = 2.03 + 0.117 \frac{S_{ice}}{T_{ice}} \tag{A1}$$

Here, S_{ice} and T_{ice} is the salinity (in ppt) and temperature (in Celsius) of sea ice, respectively. For the calculation, S_{ice} is estimated according to the empirical relationship between sea ice thickness and mean salinity from Cox and Weeks (1974) as

400 follows:

$$S_{ice} = \begin{cases} 14.24 - 19.39H, & H \le 0.4\ m \\ 7.88 - 1.59H, & H > 0.4\ m \end{cases} \tag{A2}$$

Although Trodahl et al. (2001) reported that k_{ice} depends on depth and temperature; here we do not estimate accurate thermal conductivities but attempt to examine the physical consequences within the piecewise linearity.

The comparison of calculated thermal conductivities is presented in Fig. A2. The calculated k_{ice} ranges from 1.8 W K^{-1} m^{-1} to

405 2.0 W K^{-1} m^{-1} (left two panels in Fig. A2). These values are consistent with the in-situ measurements by Pringle et al. (2006). The mean values of k_{ice} of the first part (1.96 W K^{-1} m^{-1}) and the second part (1.88 W K^{-1} m^{-1}) show almost no difference. The calculated k_{snow} ranges from 0.2 W K^{-1} m^{-1} to 1.05 W K^{-1} m^{-1} (right two panels in Fig. A2). This range is consistent with reported values in Sturm et al. (1997). The first part shows the greater and significantly spread distribution of k_{snow} compared to the second part. The mean values are 0.44 and 0.27 for the first part and second part, respectively.

410 As a significant difference is observed in k_{snow}, let us find a possible reason for this difference. To do so, we should first review the factors determining k_{snow}; they are density, temperature, and crystal structure (Sturm et al., 1997). Snow is a mixture of ice particles and air, and air has lower thermal conductivity than ice. Thus, snow with a relatively lower density including a greater portion of air should have relatively lower thermal conductivity. Besides, the thermal conductivity of ice particles depends on the temperature, and the path of heat transfer depends on the crystal structure which describes how the

415 particles are connected. The heat transfer occurs not only by conduction but also by water vapor latent heat transportation and convection through the pore spaces (Sturm et al, 2002), which are hard to be quantified explicitly. These two factors are closely related to the temperature gradient (or difference) imposed within the snow layer.

Based on this knowledge, we can infer the condition of the snow layer of the two parts. The relatively higher and varying k_{snow} of the first part would be related to the compaction process resulting in high density, and metamorphic diversity which

420 changes the crystal structure. According to Sturm et al. (2002), the value of k_{snow} of hard wind slap attains up to 0.5 W m^{-1} K^{-1}, while that of k_{snow} of depth hoar is below 0.1 W m^{-1} K^{-1}. On the other hand, the lower and nearly constant k_{snow} of the second part implies that the snow layer of the second part would consist of fresh and dry snow having relatively lower density and a relatively lower likelihood of experiencing particular metamorphism.

In summary, it is concluded that the physical properties of snow and ice can account for the piecewise linearity, based on the

425 differences in the physical properties between the first and second parts. Especially, the thermal conductivity of the snow, k_{snow}, seems to play an important role. Nevertheless, further analysis is required to fully understand this phenomenon.

Data availability

The SHEBA buoy data were obtained from NCAR/EOL (https://doi.org/10.5065/D6KS6PZ7, last access: 14 September 2019) and CRREL IMB buoy data were obtained from the CRREL-Dartmouth Mass Balance Buoy Program (http://imb-

430 crrel-dartmouth.org, last access: 14 September 2019). AASTI-v2 and SIIT data are available upon request to authors. Other data sets were obtained from NSIDC; They are OIB data (https://doi.org/10.5067/G519SHCKWQV6, last access: 10 September 2019), OIB quick look data (https://doi.org/10.5067/7Q8HCCWS4I0R, last access: 10 September 2019), CS2 data (https://doi.org/10.5067/96JO0KIFDAS8, last access: 10 September 2019), and SIC data (https://doi.org/ 10.5067/7Q8HCCWS4I0R, last access: 12 September 2019).

435 **Author contribution**

HS and BJS conceptualized and developed the methodology and HS conducted data analysis and visualization. GD and RTT gave important feedback for the algorithm development and result interpretation. GD provided AASTI data. All of the authors participated in writing the manuscript; HS prepared the original draft under supervision of BJS and GD, and BJS critically revised the manuscript.

440 **Competing interests**

The authors declare that they have no conflict of interest.

Acknowledgments

References

Alexandrov, V., Sandven, S., Wahlin, J., and Johannessen, O. M.: The relation between sea ice thickness and freeboard in

450 the Arctic, Cryosphere, 4, 373-380, doi: 10.5194/tc-4-373-2010, 2010.

Armitage, T. W. K., and Ridout, A. L.: Arctic sea ice freeboard from AltiKa and comparison with CryoSat-2 and Operation IceBridge, Geophys. Res. Lett., 42, 6724–6731, doi: 10.1002/2015GL064823, 2015.

Berg, W., Kroodsma, R., Kummerow, C. D., and McKague, D. S.: Fundamental Climate Data Records of Microwave Brightness Temperatures, Remote Sens, 10(8), 1306, doi: 10.3390/rs10081306, 2018.

455 Braakmann-Folgmann, A., and Donlon, C.: Estimating snow depth on Arctic sea ice using satellite microwave radiometry and a neural network, Cryosphere, 13, 2421–2438, doi: 10.5194/tc-13-2421-2019, 2019.

Brucker, L., and Markus, T.: Arctic-scale assessment of satellite passive microwave-derived snow depth on sea ice using Operation IceBridge airborne data, J. Geophys. Res.-Oceans, 118(6), 2892–2905, doi: 10.1002/jgrc.20228, 2013.

Comiso, J. C.: Bootstrap Sea Ice Concentrations from Nimbus-7 SMMR and DMSP SSM/I-SSMIS, Version 3, National

460 Snow and Ice Data Center, doi: 10.5067/7Q8HCCWS4I0R, 2017.

Comiso, J. C., Cavalieri, D. J., and Markus, T.: Sea ice concentration, ice temperature, and snow depth using AMSR-E data, IEEE Trans. Geosci. Remote Sens., 41(2), 243–252, doi: 10.1109/TGRS.2002.808317, 2003.

Cox, G. F. N., and Weeks, W. F.: Salinity variations in sea ice, J. Glaciol., 13(67), 109–120, doi: 10.3189/S0022143000023418, 1974.

465 Dybkjær, G., and Eastwood, S.: Validation Report for the OSI SAF High Latitude L2 Sea and Sea Ice Surface Temperature, OSI-205, Version 1.1, OSI SAF, 30 pp., 2016.

Dybkjær, G., Eastwood, S., Borg, A. L., Høyer, J., and Tonboe, R.: Algorithm theoretical basis document for the OSI SAF Sea and Sea Ice Surface Temperature L2 processing chain, OSI-205-a and OSI-205-b, Version 1.4, OSI SAF, 40 pp., 2018.

Dybkjær, G., Tonboe, R., Høyer, J., and Eastwood, S.: Arctic and Antarctic snow and ice Surface Temperatures from

470 AVHRR thermal Infrared satellite sensors, 1982-2015, 2020. (Manuscript in preparation)

Guerreiro, K., Fleury, S., Zakharova, E., Rémy, F., and Kouraev, A.: Potential for estimation of snow depth on Arctic sea ice from CryoSat-2 and SARAL/AltiKa missions, Remote Sens. Environ., 186, 339–349, doi: 10.1016/j.rse.2016.07.013, 2016.

Karlsson, K.-G., Anttila, K., Trentmann, J., Stengel, M., Meirink, J. F., Devasthale, A., Hanschmann, T., Kothe, S., Jääskeläinen, E., Sedlar, J., Benas, N., van Zadelhoff, G.-J., Schlundt, C., Stein, D., Finkensieper, S., Håkansson, N.,

475 Hollmann, R., Fuchs, P., and Werscheck, M.: CLARA-A2: CM SAF cLoud, Albedo and surface RAdiation dataset from AVHRR data - Edition 2, Satellite Application Facility on Climate Monitoring (CM SAF), doi: 10.5676/EUM_SAF_CM/CLARA_AVHRR/V002, 2017.

Kern, S., Khvorostovsky, K., Skourup, H., Rinne, E., Parsakhoo, Z. S., Djepa, V., Wadhams, P., and Sandven S.: The impact of snow depth, snow density and ice density on sea ice thickness retrieval from satellite radar altimetry: results from the

480 ESA-CCI Sea Ice ECV Project Round Robin Exercise, Cryosphere, 9, 37–52, doi: 10.5194/tc-9-37-2015, 2015.

Kilic, L., Tonboe, R. T., Prigent, C., and Heygster, G.: Estimating the snow depth, the snow-ice interface temperature, and the effective temperature of Arctic sea ice using Advanced Microwave Scanning Radiometer 2 and ice mass balance buoy data, Cryosphere, 13, 1283–1296, doi: 10.5194/tc-13-1283-2019, 2019.

Kurtz, N. T., and Farrell, S. L.: Large-scale surveys of snow depth on Arctic sea ice from Operation IceBridge, Geophys.

485 Res. Lett., 38, L20505, doi:10.1029/2011GL049216, 2011.

Kurtz, N. T., Farrell, S. L., Studinger, M., Galin, N., Harbeck, J. P., Lindsay, R., Onana, V. D., Panzer, B., and Sonntag, J. G.: Sea ice thickness, freeboard, and snow depth products from Operation IceBridge airborne data, Cryosphere, 7, 1035–1056., doi: 10.5194/tc-7-1035-2013, 2013.

Kurtz, N. T., Galin, N., and Studinger, M.: An improved CryoSat-2 sea ice freeboard retrieval algorithm through the use of
490   waveform fitting, Cryosphere, 8, 1217–1237, doi: 10.5194/tc-8-1217-2014, 2014.

Kurtz, N. and Harbeck, J.: CryoSat-2 Level-4 Sea Ice Elevation, Freeboard, and Thickness, Version 1, National Snow and Ice Data Center, doi: 10.5067/96JO0KIFDAS8, 2017.

Kurtz, N., M. Studinger, J. Harbeck, V. Onana, and D. Yi.: IceBridge L4 Sea Ice Freeboard, Snow Depth, and Thickness, Version 1, National Snow and Ice Data Center, doi: 10.5067/G519SHCKWQV6, 2015.

495   Kwok, R., and Cunningham, G. F.: Variability of Arctic sea ice thickness and volume from CryoSat-2, Phil. Trans. R. Soc. A, 373(2045), 20140157, doi: 10.1098/rsta.2014.0157, 2015.

Kwok, R., and Markus, T.: Potential basin-scale estimates of Arctic snow depth with sea ice freeboards from CryoSat-2 and ICESat-2: An exploratory analysis, Adv. Space Res., 62(6), 1243–1250, doi: 10.1016/j.asr.2017.09.007, 2018.

Kwok, R., Cunningham, G. F., Wensnahan, M., Rigor, I., Zwally, H. J., and Yi, D.: Thinning and volume loss of the Arctic
500   Ocean sea ice cover: 2003–2008, J. Geophys. Res.-Oceans, 114(C7), C07005, doi: 10.1029/2009JC005312, 2009.

Lawrence, I. R., Tsamados, M. C., Stroeve, J. C., Armitage, T. W. K., and Ridout, A. L.: Estimating snow depth over Arctic sea ice from calibrated dual-frequency radar freeboards, Cryosphere, 12, 3551–3564, doi:10.5194/tc-12-3551-2018, 2018.

Laxon, S. W., Giles, K. A., Ridout, A. L., Wingham, D. J., Willatt, R., Cullen, R., Kwok, R., Schweiger, A., Zhang, J., Haas, C., Hendricks, S., Krishfield, R., Kurtz, N., Farrell, S., and Davidson, M.: CryoSat-2 estimates of Arctic sea ice thickness
505   and volume, Geophys. Res. Lett., 40, 732– 737, doi: 10.1002/grl.50193, 2013.

Lee, S.-M., Sohn, B.-J., and Kummerow, C. D.: Long-term Arctic snow/ice interface temperature from special sensor for Microwave imager measurements, Remote Sens., 10(11), 1795, doi: 10.3390/rs10111795, 2018.

Maaß, N., Kaleschke, L., Tian-Kunze, X., and Drusch, M.: Snow thickness retrieval over thick Arctic sea ice using SMOS satellite data, Cryosphere, 7(6), 1971–1989, doi: 10.5194/tc-7-1971-2013, 2013.

510   Markus, T. and Cavalieri, D. J.: Snow depth distribution over sea ice in the Southern Ocean from satellite passive microwave data, Antarct. Res. Ser., 74, 19–39, 1998.

Markus, T., Neumann, T., Martino, A., Abdalati, W., Brunt, K., Csatho, B., Farrell, S., Fricker, H., Gardner, A., Harding, D., Jasinski, M., Kwok, R., Magruder, L., Lubin, D., Luthcke, S., Morison, J., Nelson, R., Neuenschwander, A., Stephen, P., Popescu, S., Shum, CK, Schutz, B. E., Smith, B., Yang. Y., Zwally, J.: The Ice, Cloud, and land Elevation Satellite-2
515   (ICESat-2): Science requirements, concept, and implementation, Remote Sens. Environ, 190, 260–273, doi: 10.1016/j.rse.2016.12.029, 2017.

Maykut, G. A., and Untersteiner, N.: Some results from a time-dependent thermodynamic model of sea ice, J. Geophys. Res., 76(6), 1550–1575, doi: 10.1029/JC076i006p01550, 1971.

Perovich, D., Richter-Menge, J., and Polashenski, C.: Observing and understanding climate change: Monitoring the mass

520   balance, motion, and thickness of Arctic sea ice, CRREL-Dartmouth mass balance buoy program, http://imb-crrel-dartmouth.org, 2019.

Perovich, D., Richter-Menge, J., Tucker, W., Elder, B., and Bosworth, B.: Snow and Ice Temperature Profiles. Version 1.0. UCAR/NCAR - Earth Observing Laboratory, doi:10.5065/D6KS6PZ7, 2007.

Petty, A. A., Webster, M., Boisvert, L., and Markus, T.: The NASA Eulerian Snow On Sea Ice Model (NESOSIM) v1.0:

525   initial model development and analysis, Geosci. Model Dev., 11(11), 4577–4602, doi: 10.5194/gmd-11-4577-2018, 2018.

Pringle, D. J., Trodahl, H. J., and Haskell, T. G.: Direct measurement of sea ice thermal conductivity: no surface reduction, J. Geophys. Res.-Oceans, 111(C5), C05020, doi: 10.1029/2005JC002990, 2006.

Ricker, R., Hendricks, S., Helm, V., Skourup, H., and Davidson, M.: Sensitivity of CryoSat-2 Arctic sea-ice freeboard and thickness on radar-waveform interpretation, Cryosphere, 8, 1607–1622, doi: 10.5194/tc-8-1607-2014, 2014.

530   Rostosky, P., Spreen, G., Farrell, S. L., Frost, T., Heygster, G., and Melsheimer, C.: Snow depth retrieval on Arctic sea ice from passive microwave radiometers – improvements and extensions to multiyear ice using lower frequencies, J. Geophys. Res.-Oceans, 123(10), 7120–7138, doi: 10.1029/2018JC014028, 2018.

Sturm, M., Holmgren, J., König, M., and Morris, K.: The thermal conductivity of seasonal snow, J. Glaciol., 43(143), 26–41, doi: 10.3189/S0022143000002781, 1997.

535   Sturm, M., Perovich, D. K., and Holmgren, J.: Thermal conductivity and heat transfer through the snow on the ice of the Beaufort Sea, J. Geophys. Res., 107(C21), 8043, doi: 10.1029/2000JC000409, 2002.

Tonboe, R. T., Pedersen, L. T., Haas, C.: Simulation of the CryoSat-2 satellite radar altimeter sea ice thickness retrieval uncertainty, Can. J. Remote Sens., 36(1), 55–67, doi: 10.5589/m10-027, 2010.

Trodahl, H. J., Wilkinson, S. O. F., McGuinness, M. J., and Haskell, T. G.: Thermal conductivity of sea ice; dependence on

540   temperature and depth, Geophys. Res. Lett., 28(7), 1279–1282, doi: 10.1029/2000GL012088, 2001.

Warren, S. G., Rigor, I. G., Untersteiner, N., Radionov, V. F., Bryazgin, N. N., Aleksandrov, Y. I., and Colony, R.: Snow depth on Arctic sea ice, J. Climate, 12(6), 1814–1829, doi: 10.1175/1520-0442(1999)012<1814:SDOASI>2.0.CO;2, 1999.

Webster, M. A., Rigor, I. G., Nghiem, S. V., Kurtz, N. T., Farrell, S. L., Perovich, D. K., and Sturm, M.: Interdecadal changes in snow depth on Arctic sea ice, J. Geophys. Res.-Oceans, 119(8), 5395–5406, doi: 10.1002/2014JC009985, 2014.

545   Wingham, D. J., Francis, C. R., Baker, S., Bouzinac, C., Brockley, D., Cullen, R., Chateau-Thierry, P., Laxon, S. W., Mallow, U., Mavrocordatos, C., Phalippou, L., Ratier, G., Rey, L., Rostan, F., Viau, P., and Wallis, D. W.: CryoSat: a mission to determine the fluctuations in Earth's land and marine ice fields, Adv. Space Res., 37(4), 841–871, doi: 10.1016/j.asr.2005.07.027, 2006.

Zhou, L., Xu, S., Liu, J., and Wang, B.: On the retrieval of sea ice thickness and snow depth using concurrent laser altimetry

550   and L-band remote sensing data. Cryosphere, 12(3), 993–1012, doi: 10.5194/tc-12-993-2018, 2018.

Zwally, H. J., Schutz, B., Abdalati, W., Abshire, J., Bentley, C., Brenner, A., Bufton, J., Dezio, J., Hancock, D., Harding, D., Herring, T., Minster, B., Quinn, K., Palm, S., Spinhirne, J., and Thomas, R.: ICESat's laser measurements of polar ice, atmosphere, ocean, and land, J. Geodyn., 34, 405–445, doi: 10.1016/S0264-3707(02)00042-X, 2002.

Zygmuntowska, M., Rampal, P., Ivanova, N., and Smedsrud, L. H.: Uncertainties in Arctic sea ice thickness and volume: 555   new estimates and implications for trends, Cryosphere, 8(2), 705–720, doi: 10.5194/tc-8-705-2014, 2014.

Table 1. Information on the measurement sites of buoys whose observations were used in this study.

Name		Deployment Location	Ice Type	Initial Snow Depth [m]	Initial Ice Thickness [m]
CRREL	2010F	Beaufort Sea	Multi-Year	0.25	1.97
	2011M	Central Arctic	Multi-Year	0.07	1.67
	2012G	Central Arctic	First-Year	0.16	1.41
	2013F	Beaufort Sea	Multi-Year	0.00	1.40
	2013G	Beaufort Sea	Multi-Year	0.00	1.40
	2014G	Beaufort Sea	Multi-Year	0.10	1.08
	2014I	Beaufort Sea	Multi-Year	0.23	1.32
SHEBA	Q2	Beaufort Sea	Multi-Year	0.06*	1.75*
	PIT	Beaufort Sea	Multi-Year	0.12*	2.01*
	BALT	Beaufort Sea	First Year	0.07*	1.40*
	R4	Beaufort Sea	Second-Year Ridge	0.09*	4.23*
	SEA	Beaufort Sea	Ponded Area	0.10*	1.54*

560 *The initial snow depth and ice thickness of the SHEBA sites are average values of all thickness gauge measurements in the corresponding site because there was one thermistor string but several thickness gauges in each measurement site

565

Table 2. Coefficients of the regression equation for averaging periods of 1, 7, 15, and 30 days. a_1, b_1, a_2, b_2, and x_0 are given in Eq. (8).

Averaging Periods	a_1	b_1	a_2	b_2	x_0
1 day	0.166	0.047	0.050	0.263	1.864
7 days	0.179	0.028	0.053	0.254	1.796
15 days	0.180	0.034	0.029	0.339	2.022
30 days	0.185	0.022	0.076	0.214	1.769

The Cryosphere
Discussions

Open Access

EGU
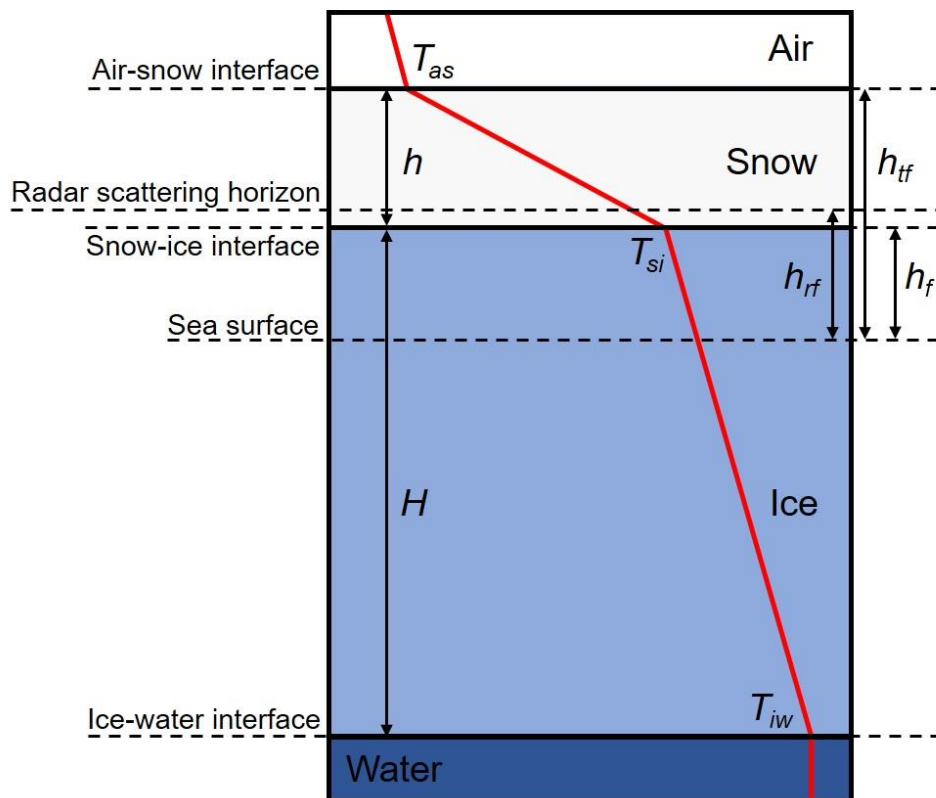
Figure 1. Schematic diagram of a typical snow–ice system during winter. Snow depth (h), ice thickness (H), total freeboard (h_{tf}), radar
570   freeboard (h_{rf}), and ice freeboard (h_f) are indicated. The red line denotes a typical temperature profile with air–snow interface temperature
(T_{as}), snow–ice interface temperature (T_{si}) and ice–water interface temperature (T_{iw}).

The Cryosphere
Discussions

Open Access

EGU
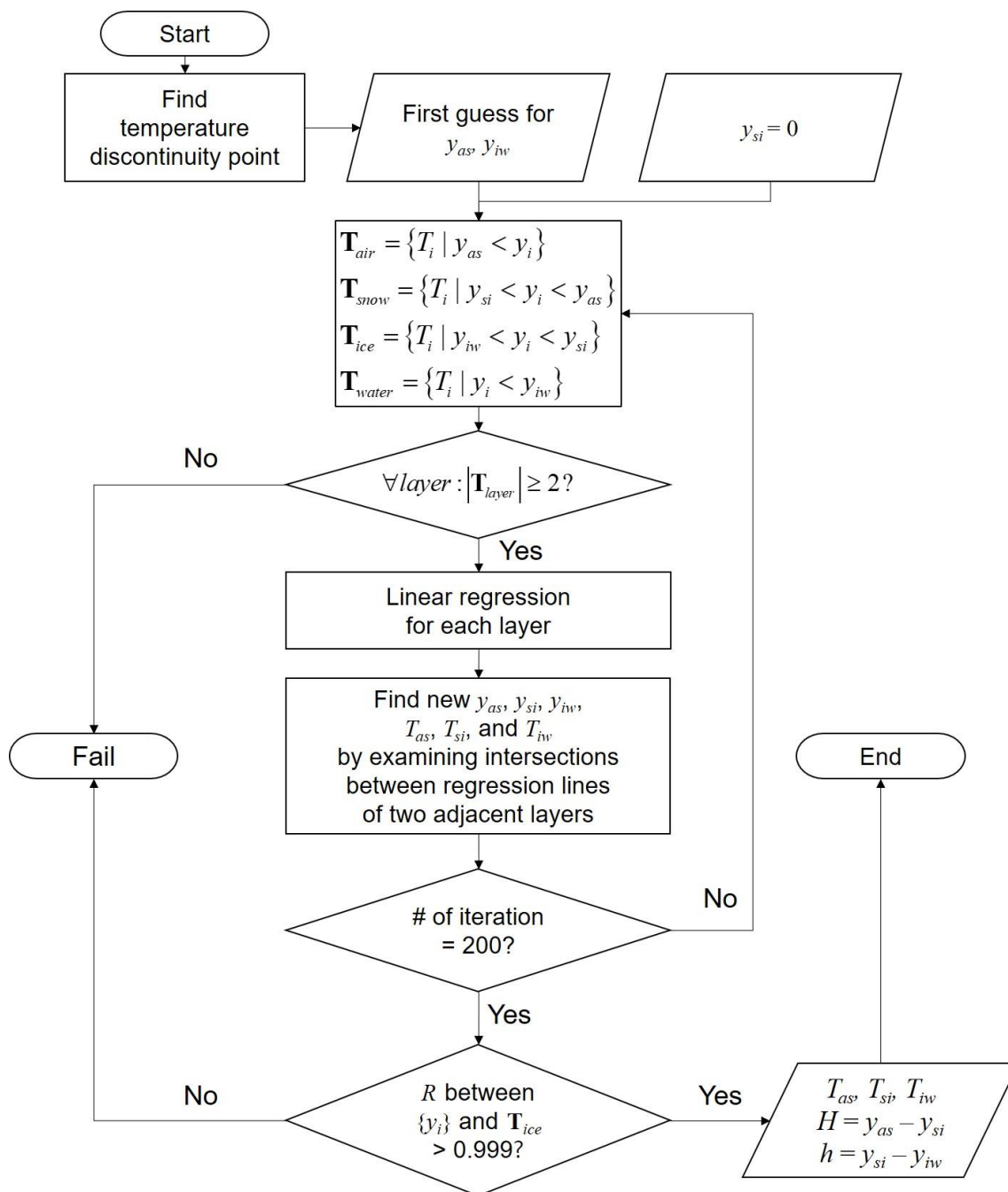
Figure 2. The flow chart of the interface searching algorithm. y_i and T_i denote the position and temperature of a data point in the temperature profile. y_{as}, y_{si}, and y_{iw} denote the position of the interfaces, and $\mathbf{T}_{layer}$ denotes a set of temperature data points.

575

22
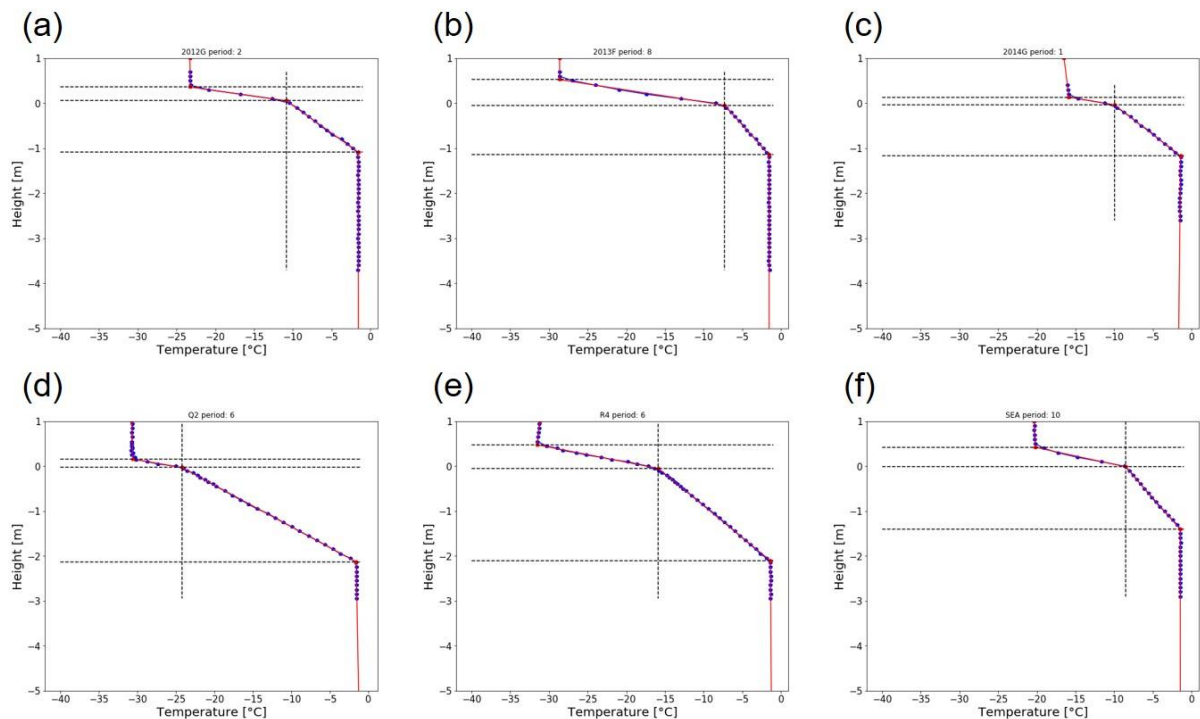
Figure 3. Examples of interface searching results with an averaging period of 15 days: (a) 2012G period 2, (b) 2013F period 8, (c) 2014G period 1, (d) Q2 period 6, (e) R4 period 6, and (f) SEA period 10. The period number is equivalent to the number of time averaging bin. Blue dots are buoy-measured temperature profiles and red lines are regression lines. Black dashed lines indicate the intersections between adjacent regression lines.
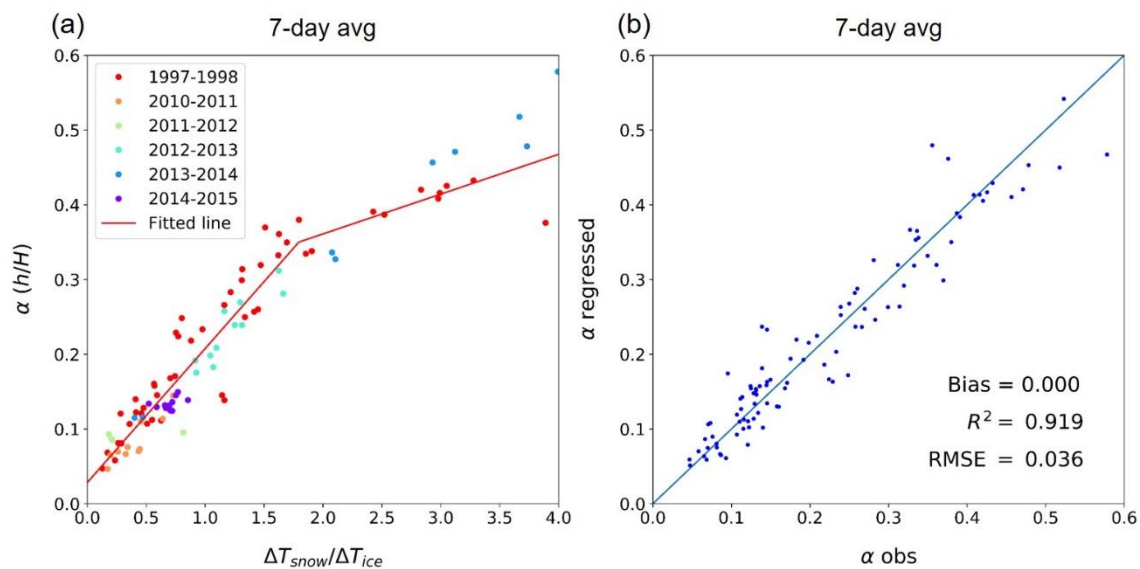
Figure 4. (a) Scatterplots of the temperature difference ratio of the snow and ice layer ($\Delta T_{snow}/\Delta T_{ice}$) and the snow–ice thickness ratio (α).
Color denotes collected year of buoy data. The red lines are the regression lines (defined in Eq. (8)). (b) The scatter plot of observed and regressed α.

The Cryosphere
Discussions
Open Access
EGU
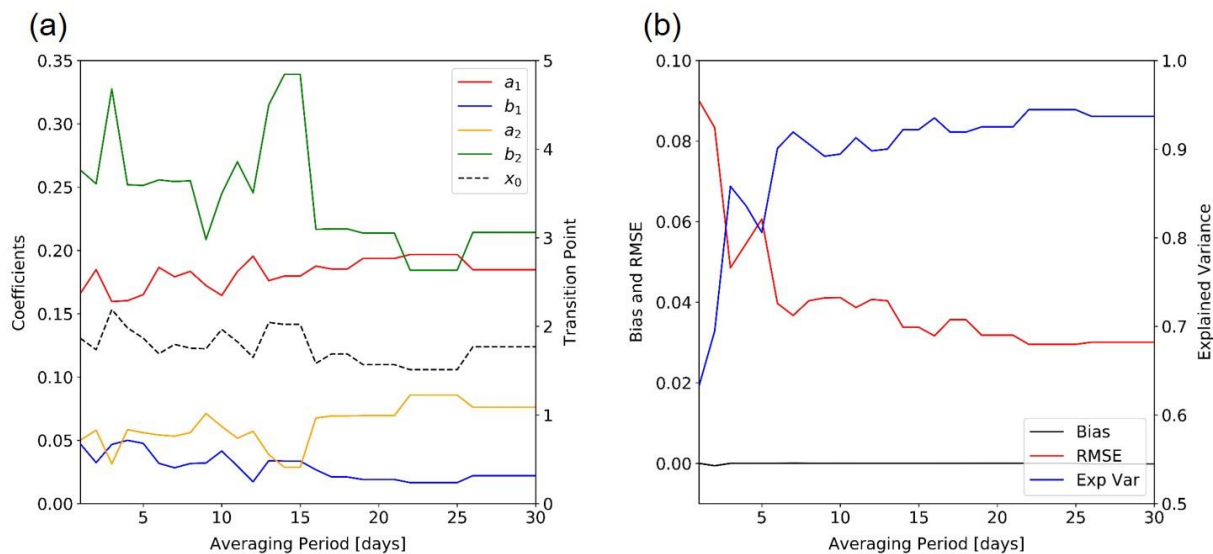
Figure 5. (a) The regression coefficients (a_1, b_1, a_2, b_2) in Eq. (8) and (b) the error statistics of the regression with averaging periods from 1 to 30 days.
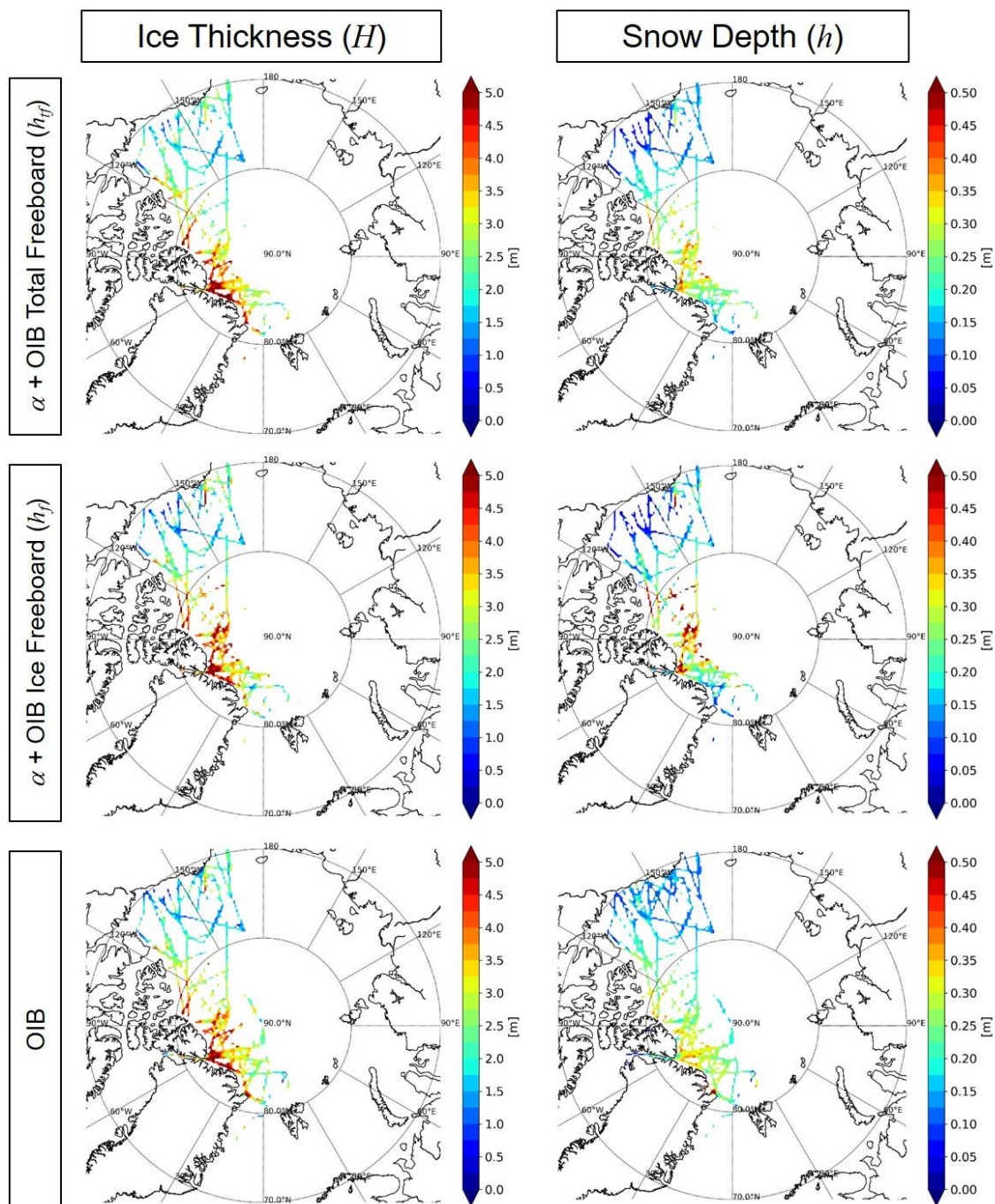
Figure 6. Simultaneously retrieved ice thickness and snow depth from OIB total/ice freeboard in March of the 2011–2015 period. Corresponding OIB products are at the bottom.
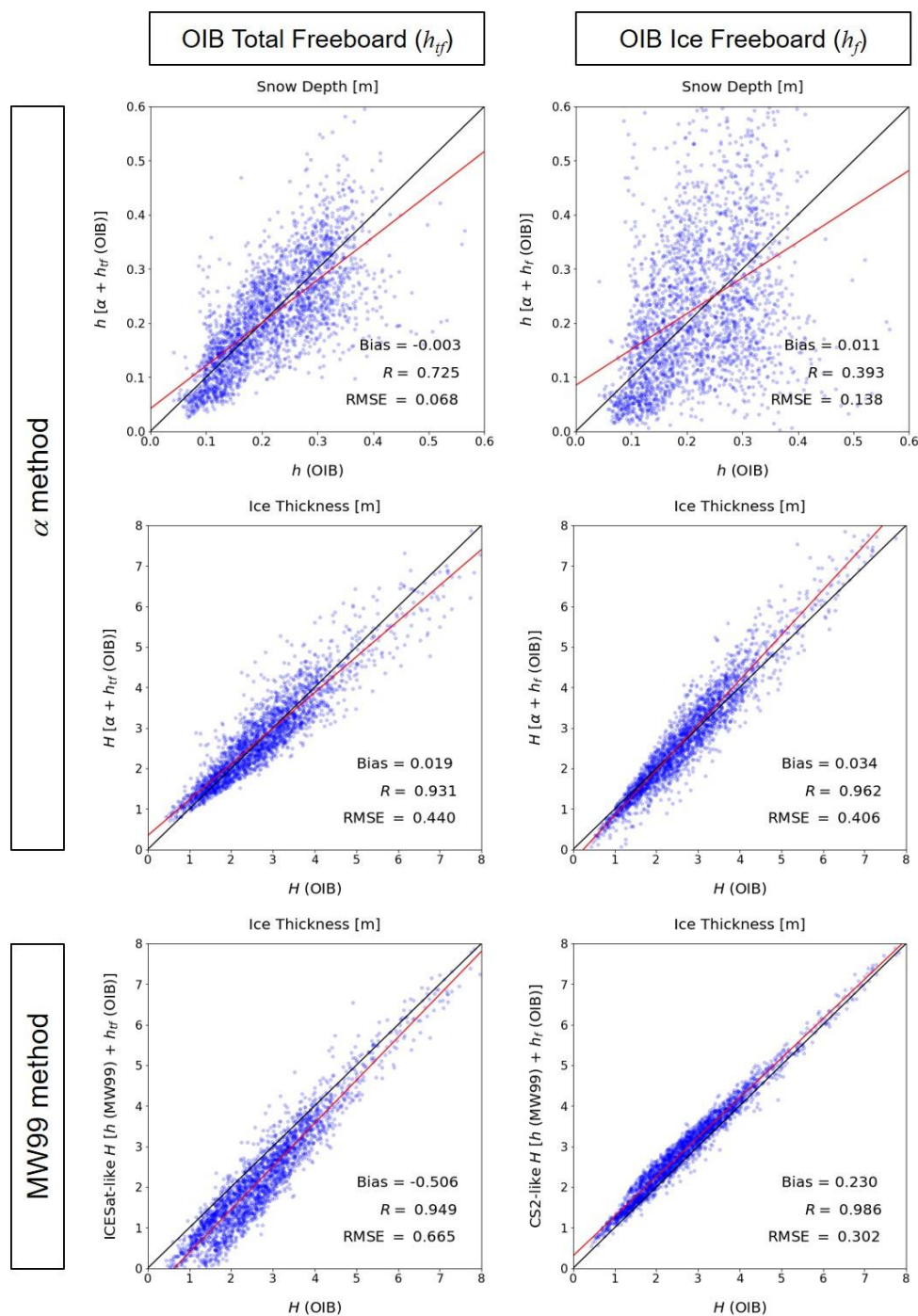
Figure 7. Scatter plots between OIB products and the simultaneously retrieved snow depth and ice thickness from OIB total/ice freeboards during the March 2011–2015 period. Corresponding ice thicknesses estimated from MW99 snow depth are in the third row. The red lines are linear regression lines.
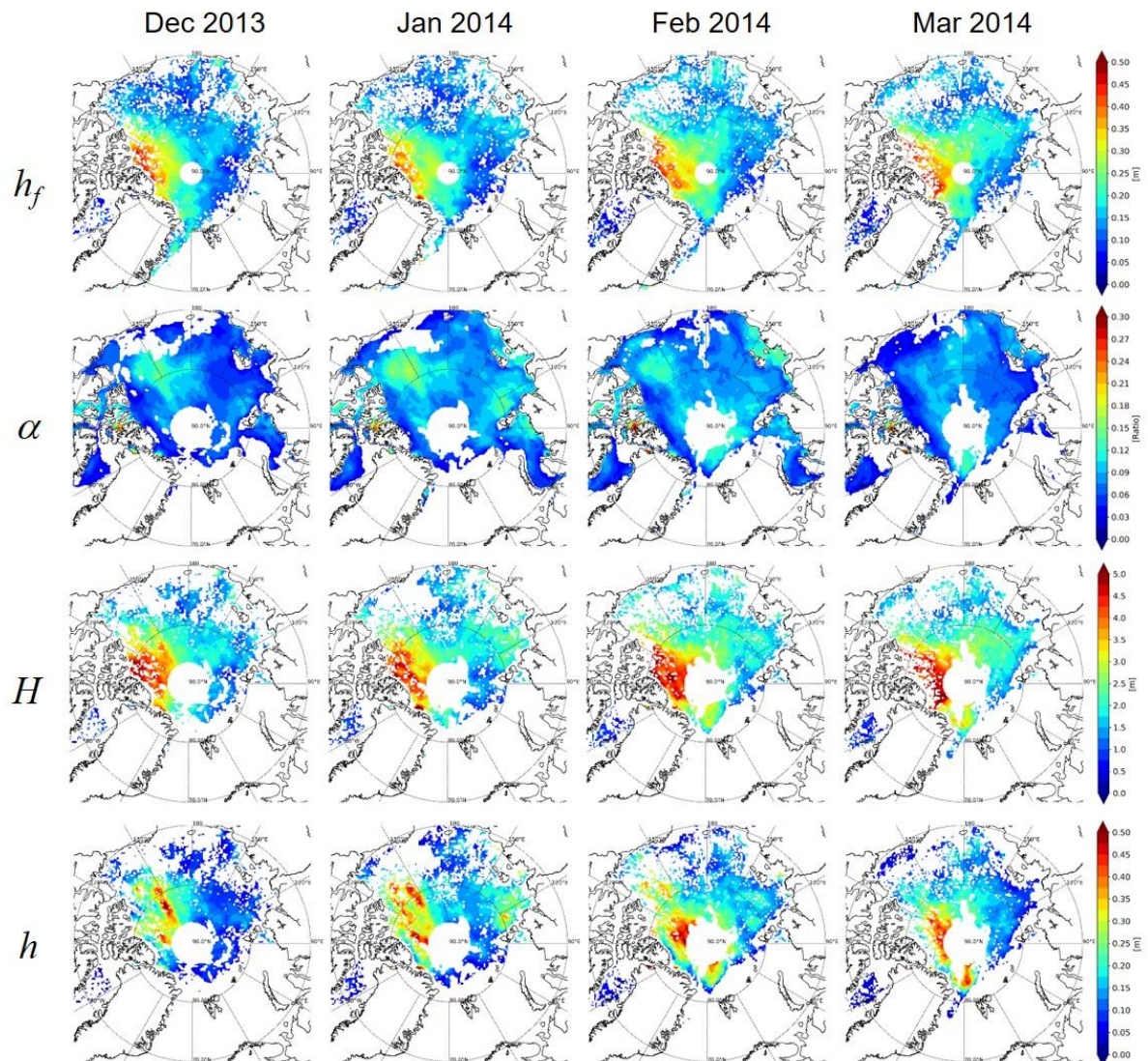
Figure 8. Geographical distributions of observed CS2 ice freeboard (h_f) and estimated snow–ice thickness ratio (α), ice thickness (H), and snow depth (h) from December 2013 to March 2014.
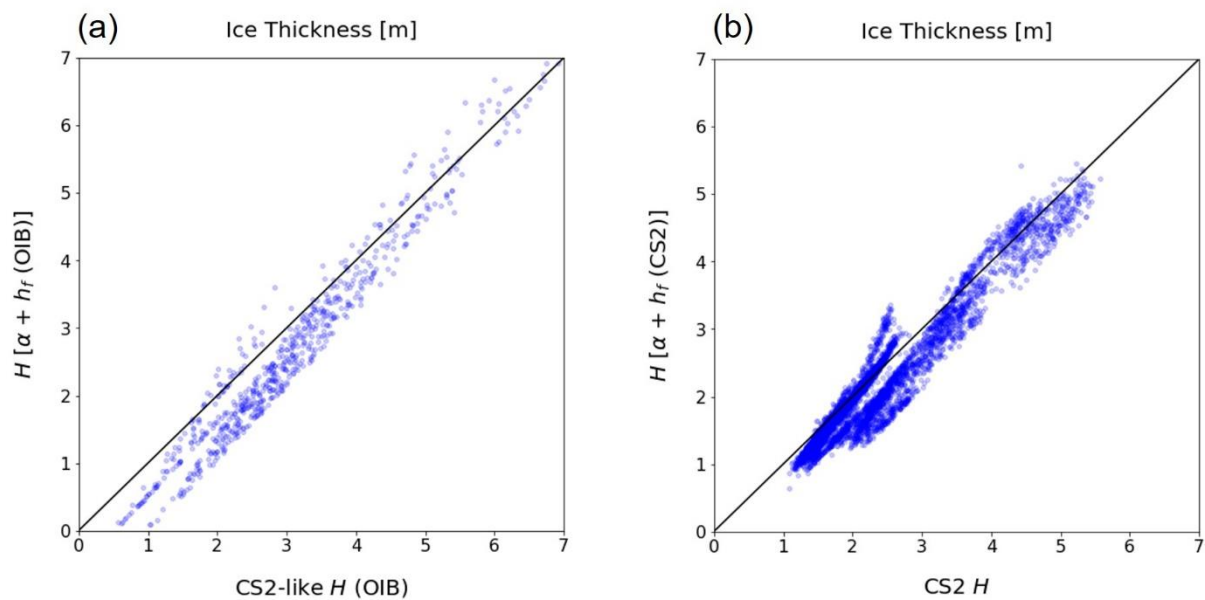
605

Figure 9. Comparison of retrieved ice thickness between the MW99 method and the α method using (a) OIB ice freeboard and (b) CS2 freeboard on March 2014. CS2-like H (OIB) denotes the ice thickness estimated from the MW99 snow depth and OIB ice freeboard.
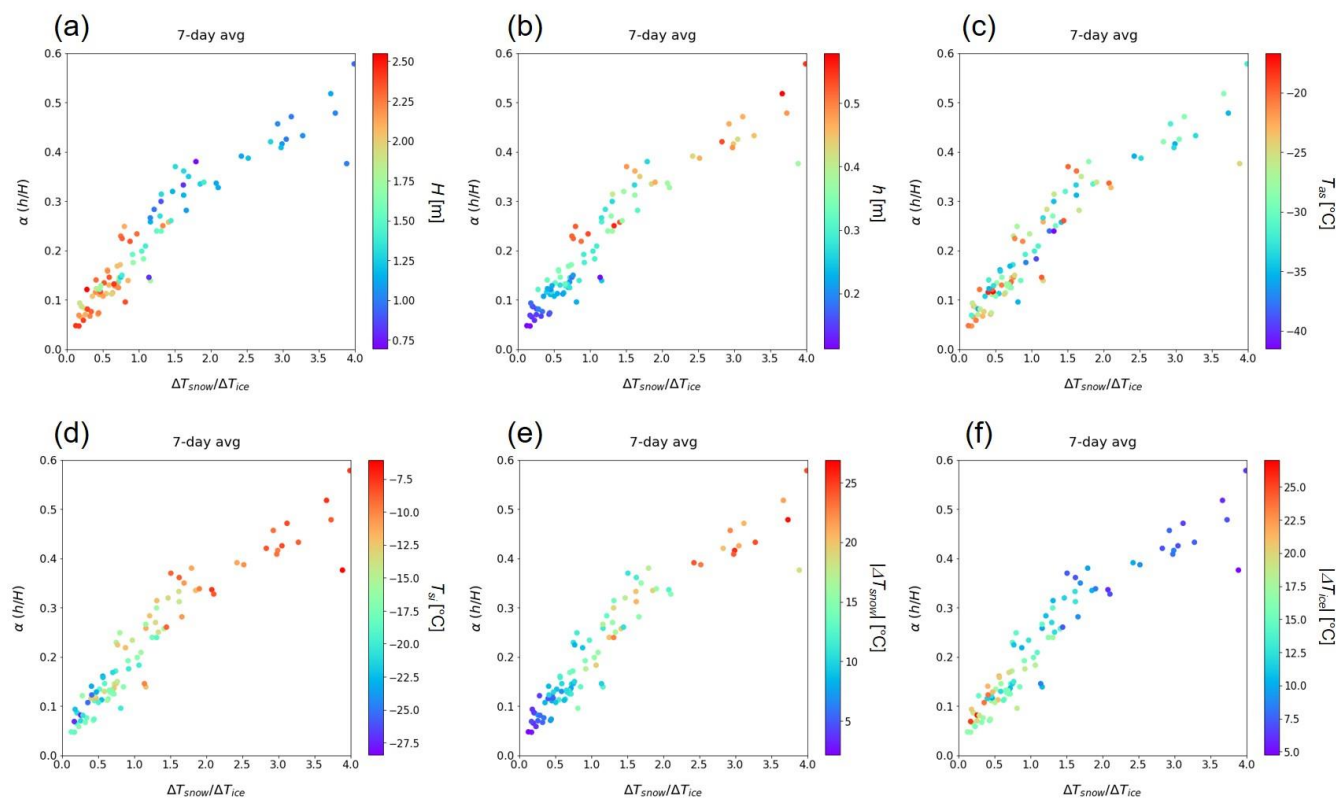
610

Figure A1. Distribution of physical variables on scatterplots of the temperature difference ratio of snow and ice layer ($\Delta T_{snow}/\Delta T_{ice}$) and the snow–ice thickness ratio (α). Color denotes the value of physical variables: (a) ice thickness (H), (b) snow depth (h), (c) air–snow interface temperature (T_{as}), (d) snow–ice interface temperature (T_{si}), (e) temperature difference within snow layer ($|\Delta T_{snow}|$), and (f) temperature difference within ice layer ($|\Delta T_{ice}|$).
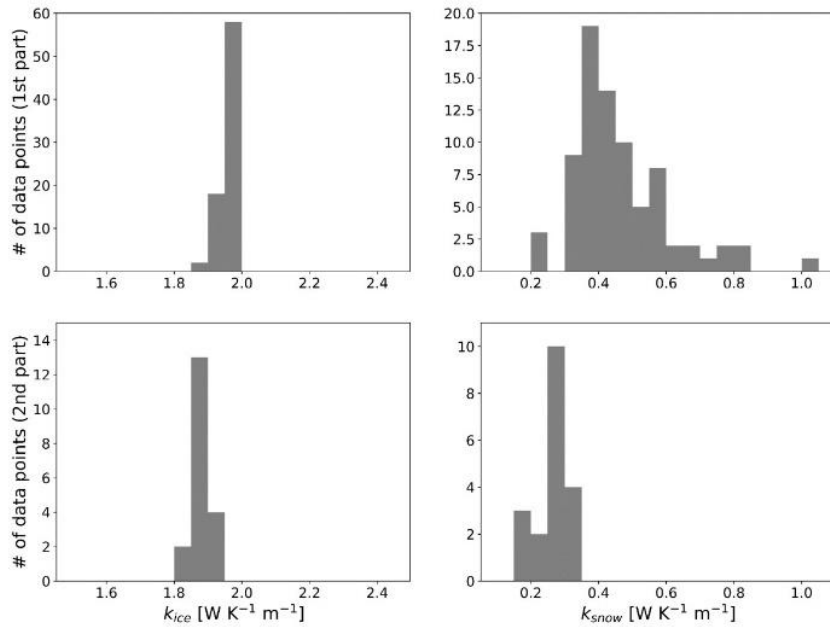
615

Figure A2. Histogram of estimated (left column) k_{ice} and (right column) k_{snow}. The top and bottom row denote the first and the second part, respectively. The size of the bins is 0.05 W K^{-1} m^{-1}.